

[doi:10.25143/rsu_morf-stud-conf_2021_abstracts](https://doi.org/10.25143/rsu_morf-stud-conf_2021_abstracts)



RĪGA STRADIŅŠ
UNIVERSITY

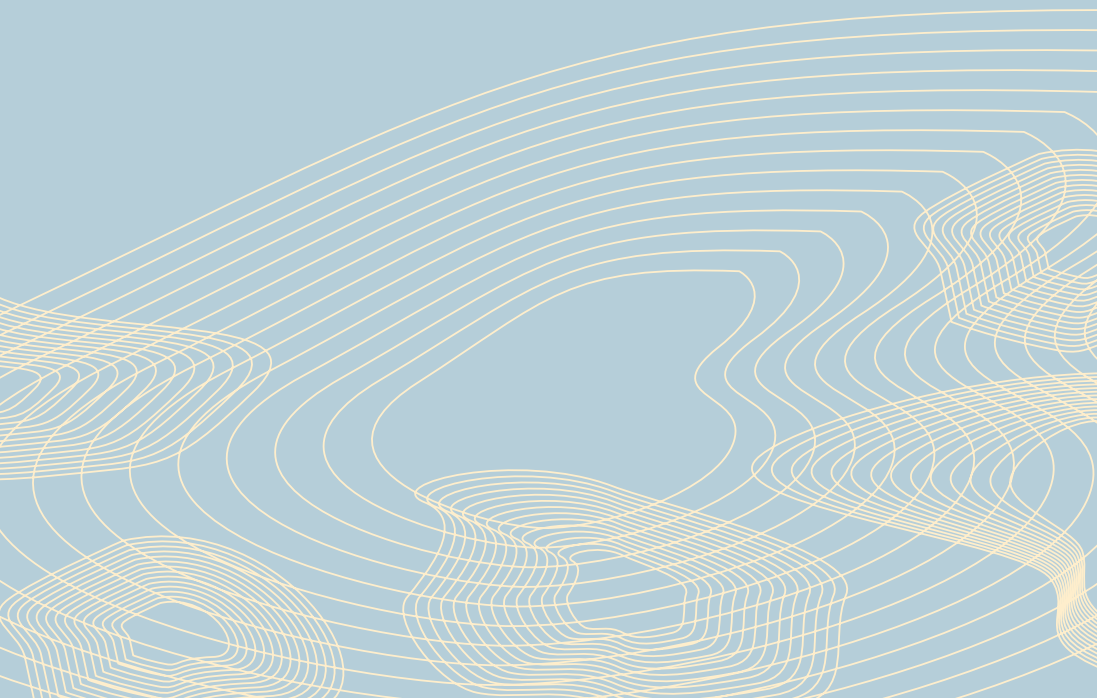
OPEN TO THE WORLD

INSTITUTE OF ANATOMY
AND ANTHROPOLOGY

**XXVI Student International Conference of
MORPHOLOGY SCIENCES**

6 May 2021 Rīga

Abstracts Book





RĪGA STRADIŅŠ
UNIVERSITY

OPEN TO THE WORLD

INSTITUTE OF ANATOMY
AND ANTHROPOLOGY

**XXVI Student International Conference of
MORPHOLOGY SCIENCES**

6 May 2021 Rīga

Abstracts Book

Rīga Stradiņš University
Institute of Anatomy and Anthropology
Kronvalda boulevard 9
Rīga, LV-1010
Phones: 67326526, 67320862

Organisers of the conference:
Professor M. Pilmane
Assoc. Professor Dz. Kažoka
Office Secretary D. Enkuzena

All abstracts have been reviewed

XXVI Student International Conference of Morphology Sciences
[6 May, 2021, Riga]: Abstracts Book. Riga: RSU, 2021. 44 p.
https://doi.org/10.25143/rsu_morf-stud-conf_2021_abstracts

Proof reader: Jānis Zeimanis
Layout: Ilze Stikāne

No. IPD-1266

© Rīga Stradiņš University, 2021
Dzirciema street 16, Rīga, LV-1007

ISBN 978-9934-563-84-3 (printed)
ISBN 978-9934-563-85-0 (electronic)

Contents

The Difference of Anosmia in the Case Of SARS-COV-2 and Other Infections <i>N. Atiya</i>	5
Modelling of Distal Humerus Osteosarcoma Using 3D Printing Techniques <i>L. Banceviča</i>	7
The Intramuscular Hemangioma of the Thigh: a Case Report and Review of Literature <i>Z. Bodniece, U. Zelmene</i>	9
Evaluation of Foot Medial Longitudinal Arch Deformities Using the Calcaneal Inclination Angle <i>V. Boikova</i>	11
Illustration of FIGO Classification of Uterine Fibroids <i>E. Bozzotto</i>	12
Celiac Plexus and Its Block: Anatomical Review, Indications and Comparison of Techniques <i>L. Gasiņa</i>	14
Architecture of Heart Valve Vegetation in Infective Endocarditis Patients Examined Using Transmission Electron Microscopy <i>N. R. Goldiņš</i>	16
Frequently Reported Drugs: Inducers of the Phototoxicity <i>A. Grabčika</i>	17
Anatomical Variation of the Greater Palatine Foramen in a Digital Cranium Collection <i>F. Kipp</i>	19
Pubic Arch Angle as a Predictive Factor of Childbirth Outcome <i>K. Koliste, V. Boikova</i>	20
Local Defence System in Healthy Lungs <i>E. Lohova</i>	22
Anatomical Variants of the Internal Jugular Vein and Its Importance in Vascular Access for Catheterisation <i>A. Makarova, E. Junusova</i>	24

Anatomical Aspects of Topography and Clinical Significance of the Carpal Tunnel <i>P. M. L. Mardin, L. L. Striķe</i>	25
Comparison of Three Types of Central Venous Catheterisation Places <i>J. Muravjova, A. Semjonova</i>	27
Surgical Access to Middle Cerebral Artery in Case of Aneurysm <i>R. Puriņš</i>	28
Anatomical Macrostructures Related to Development and Expression of Glioblastoma Multiforme (GBM): Literature Review <i>D. Semke</i>	30
Evaluation of Different Tissue Factors and Apoptosis in Primary Obstructive Megaureter Tissue <i>I. Siņičins</i>	31
Morphological Analysis of Alcohol-induced Destruction in Liver Parenchyma <i>M. Skultecka</i>	33
Anatomical Aspects of Facial Filler Injection <i>J. Smirnova, A. Krauß</i>	34
Ki-67 and PTEN Expression in Endometrial Hyperplasia and Cancer <i>E. Strautmane</i>	35
Geometrical Variations of Circle of Willis <i>A. Ševčenko</i>	37
Access to the Ventral Pontomesencephalic Region of the Brain Through the Different Intracranial Corridors <i>L. Unzule</i>	38
Topography and Clinical Importance of Some Intracranial Triangles in the Cavernous Sinus, Middle Fossa and Sellar Region <i>L. Unzule</i>	40
Variations and Clinical Effects of Aortic Coarctations <i>P. M. Vimba</i>	42
Authors Index	44

The Difference of Anosmia in the Case Of SARS-COV-2 and Other Infections

Noy Atiya, Faculty of Medicine, 2nd year

Supervisor – *Dr. med.*, Associate Professor Dzintra Kažoka

Introduction. Changes of the smell and taste are recognised as some of the cardinal symptoms of COVID-19 (*Butoft, 2020*). Symptoms of SARS-CoV-2 (fever, weakness and cough) can be associated with flu or other infections, but anosmia induced by SARS-CoV-2 has several unique features. Key to understanding such differences may lie in the frequency of variants in the virus entry proteins. The destructive power and the exact mechanism of the SARS-CoV-2 on the olfactory system remain unknown (*Meng et al., 2020*).

Aim. The aims of this study were to focus on structures of olfactory nerve, the difference between anosmia in case of SARS-COV-2 and other infections, and to discuss the prevalence of this common symptom in SARS-COV-2 patients, according to the review of literature.

Materials and Methods. In part 1 of the study, medical literature in human anatomy, histology and physiology was used for detection of structures of olfactory system. The width and length of olfactory tract, bulb and trigonum of both sides were measured on three human brains, using digital caliper. Materials were provided by Laboratory of Anatomy of Department of Morphology at the Institute of Anatomy and Anthropology. In part 2 of the study, the differences between types of anosmia were clarified by broadly searched literature databases, including *PubMed*, *Google Scholar* and *Web of Science*.

Results. There was no significance in differences of length or width of the olfactory nerves that were measured in brains. From the pathophysiology point of view, the olfactory neurons are in high risk to be damaged because the increase of viral load in the nasal cavity. Anosmia in case of SARS-COV-2 appears sudden and severe compared to other infections which mostly happen gradually and might be not fully anosmia (hyposmia). Olfactory dysfunction (OD) might be caused after upper respiratory tract infections (URI). *Touïsserkani et al. (2020)* classified OD into conductive (physical blockage of airflow to olfactory mucosa) or sensorineural types (disruption of the olfactory neural signalling pathway). URI is the most common cause of OD. Human rhinovirus, parainfluenza virus type 2, picornavirus, Epstein-Barr virus and human coronavirus have all been

observed to cause postviral OD. The virus might damage the olfactory epithelium and change the number and function of its receptors (*Suzuki et al., 2007*).

Anosmia caused by SARS-COV has been reported during the SARS epidemic (*Hwang, 2006*). In Germany there were approximately 60% patients that were indicated of reduction of smell and taste caused by SARS-COV-2 (*Streeck, 2020*). Portal of entry of SARS-COV-2 in case of causing anosmia is predicted to be by invading the olfactory mucous layer and accumulate in sustentacular cells. In these cells there is an abundant expression of ACE2 and TMPRSS2 proteins which are the entry proteins of the virus. Mature olfactory receptor neurons do not express ACE2 or TMPRSS2 or in lesser amount, which might explain why these cells are not or are less infected with SARS-COV-2 (*Baxter et al., 2020*). Replacement of the sustentacular cells might take longer because from stem cell it produced firstly immature olfactory receptor neurons and only later, they turn to mature. It is still unclear how mature olfactory receptor neurons (mORN) are dying or damaged if they do not express the entry proteins of the virus (*Bryche et al., 2020; Sia et al., 2020*).

In case of flu or other infections the reason for anosmia can cause nasal obstruction or congestion, or irritation to the mucus membrane lining (*Cafasso, 2019*). Thus, the odors cannot transfer to the olfactory receptor neurons (*Doty et Mishra, 2001; Hummel et al., 2017*). Other possible reason is brain or nerve damages. If the damage is to the olfactory receptor neurons, it causes to block the transmission of smell sensation. If the neurons are damaged in the brain, the sensation of the smell is changed.

Conclusions.

2. There is a difference regarding anosmia caused by SARS-COV-2 and anosmia caused by other infections such as common flu.
3. The mechanisms of COVID-19 related OD are different from those seen in other infections and may reflect a specific involvement at the level of central nervous system.
4. In the future studies to assess the prevalence of anosmia and neuroanatomical changes can be useful to understand these mechanisms.

Modelling of Distal Humerus Osteosarcoma Using 3D Printing Techniques

Lilija Banceviča, Faculty of Medicine, 2nd year

Supervisors – *Dr. med.*, Associate Professor Dzintra Kažoka;

Dr. Anna Valaine (Department of Hematology and Oncology,
Children's Clinical University Hospital)

Introduction. Among all bone malignancies and tumours, the most frequent is osteosarcoma, which is more common among children and teenagers (*Prater et al.*, 2020). The most usual locations of osteosarcoma are the distal femur, proximal humerus and proximal tibia. Distal humerus is a very rare location for osteosarcoma. It is usually treated by neoadjuvant chemotherapy followed by amputation of upper limb to the proximal epiphysis of the humerus (*Arora et al.*, 2020). Due to destructive and aggressive malignant features, treating osteosarcoma may be challenging. Nowadays 3D printing techniques are practised more frequently in orthopaedic oncological surgery by using MRI and CT scans of the tumour affected part of the body to establish precise resection of the tumour and necessary limb part replacement (*Liciu et al.*, 2018).

Aim. The aim of the study was to simulate osteosarcoma of the distal humerus and make a 3D model of the treated distal humerus with the cubital joint.

Materials and Methods. “*Complete Anatomy 2021*” app was used to visualise anatomical structures of the upper limb. “*Meshmixer*” software and “*Sketchfab*” were used for simulation of tumour affected distal humerus and creating a model of treated osteosarcoma. Prototype for model creation was taken from “*World Journal of Orthopedics*” (*Vasiliadis et al.*, 2013). The prototype of low-grade stage IB central osteosarcoma of the distal femur was remodelled on the distal part of humerus.

3D printer and material for printing the model in distal humerus replacement procedure were provided by Laboratory of Anatomy of Department of Morphology at the Institute of Anatomy and Anthropology. Arm and forearm skin, muscles, then veins, nerves and arteries of the upper limb were virtually dissected using “*Complete Anatomy 2021*” app for visualisation of untreated and treated tumour.

After the creation of models of treated and untreated osteosarcoma, these models were printed by using a 3D printer. Measurements of the tumour model were made to establish precise resection of the tumour by using a caliper, and part of humerus for replacement with 3D printed part (prosthesis) was prepared. The volume of osteogenic osteosarcoma on the 1st model was calculated by using

$V = (W (2) \times L)/2$, where V is tumor volume, W – width, L – length (*Faustino-Rocha et al., 2013*).

Results. In this study, a case of distal humerus osteosarcoma in the anterior part of the left upper extremity bone was simulated. In digital platform, skin layer was virtually removed, biceps brachii muscle and cephalic vein, brachial muscle and musculocutaneous nerve were dissected. Basilic vein, brachial veins, brachial artery, superior collateral ulnar artery, collateral veins of elbow joint, median nerve, posterior and anterior branches of medial antebrachial cutaneous nerves were moved aside medially, and afterwards, brachioradial muscle was dissected. The collateral radial artery, recurrent radial vein and radial nerve were moved laterally to make clear the surface of anterior part of distal humerus.

Afterwards, two models of tumour affected and treated post-osteosarcoma of the distal humerus were prepared for 3D printing. The 1st model or the osteogenic osteosarcoma was modelled on distal humerus using “*spikes*” and “*rebussmooth*” brushes for bone tumour appropriate texture. Stage of osteosarcoma was detected. The length of tumour was 6.08 cm, the width of tumour was 1.87 cm, and tumour depth was 0.89 cm. The volume was 10.63 cm³. The 2nd model of the treated distal humerus was created with removed osteosarcoma.

Conclusions.

1. Complications of damaging soft tissues, blood vessels and nerves of upper and lower limbs are expected in the surgical treatment of distal humerus osteosarcoma.
2. Two 3D printed models were used to provide precise information regarding surgical procedure simulation before and after resection of the tumour.
3. 3D printing technologies can be used as an alternative method of surgically treating osteosarcoma of distal humerus, and this procedure may benefit from preserving the cubital joint functions, an increasing surgical accuracy and lowering rate of tumour-related complications and metastases.

The Intramuscular Hemangioma of the Thigh: a Case Report and Review of Literature

Zane Bodniece, Una Zelmene, Faculty of Medicine, 3rd year
Supervisor – *Dr. med.*, Associate Professor Dzintra Kažoka

Introduction. A hemangioma is a tumour that originates from vascular tissue and may develop in almost any part of the body, including the skin, subcutaneous tissue, muscle, splanchnic tissue and bone. The skeletal muscle hemangiomas are uncommon soft tissue tumours. More than 90% are misdiagnosed initially (Scott, 1957). The intramuscular hemangiomas account for approximately 0.8% of all benign soft tissue tumours. They present as chronic pain and swelling in a muscle with or without a history of trauma.

Aim. The aims of the study were: to investigate a case report from 2006; to prepare literature review of similar case reports; to improve anatomical and clinical knowledge about intramuscular hemangioma and to study this pathology as a differential diagnosis in musculoskeletal pain.

Materials and Methods. One case report was used in the study: in 2006 a six-year-old girl presented with a mass in the right lower leg (distal, 1/3 anterior, lateral surface) and with mild pain. The mass restricted movement and caused discomfort. The blood puncture was performed twice. USG in the inpatient brought suspicion of a semi-organising hematoma; however, a differentiation from other etiological changes was suggested. Surgery under general anesthesia was performed – an inspection of the formation in the right thigh, revealed that clinically it resembled a cavernous hemangioma leaving the muscle tissue. The hemangioma was exfoliated using electrocoagulation, the sutures were placed on the muscle fibers and the wound was closed. The wound was closed with an intracutaneous suture.

In study process a literature search was performed using *PubMed*, *ScienceDirect*, *NCB*, *Elsevier* and *AccessMedicine*. The relevant articles and referenced sources were reviewed for additional articles that discussed the epidemiology, pathophysiology, investigation and management of intramuscular hemangiomas. Similar clinical cases were observed in patients under 18 years of age with the affected area – the thigh. These cases were analysed by age, gender, affected site, clinical symptoms, diagnostic and treatment methods.

Results. 7 clinical cases of patients under the age of 18 years were analysed, 5 of which were males and 2 were females. The younger age groups are most frequently affected with 85% of cases under the age of 30 years. 5 patients were reported to have swelling, 2 – muscle stiffness. All of them noted pain in

the affected area, as well as limited movement. Intramuscular hemangiomas are usually asymptomatic at the initial stage. Clinically, intramuscular hemangiomas usually present with pain (55%) and swelling, with symptoms usually lasting one to five years (range 0–70 years). A mass is found in 98% of cases (Ferguson, 1972). The mass may be pulsatile or have a bruit. In 2 cases the localisation was in the supra-patellar area, 5 were related to the *m. quadriceps femoris* within any part of it (*m. vastus medialis*, *m. vastus lateralis* or *m. rectus femoris*). The anatomical distribution of hemangiomas affected the lower limb in 32%, the head and neck in 27%, the upper limb in 24% and the trunk in 17%. The thigh is the most common intramuscular site in 17–19% (Jenkins, 1932; Scott, 1957). Wild *et al.* (2000) found the quadriceps to be affected in five out of 11 cases of intramuscular hemangioma. In 72% of cases, it was found that one muscle with an average diameter of 5.5 cm was involved. Watson *et al.* (1940) found that 16% of all the hemangiomas had more than one site.

The etiology of cavernous hemangioma may be congenital, trauma or hormone imbalance-related, but the exact etiology is not clearly defined. X-ray and ultrasound examination were used in all the cases as diagnostic methods. Magnetic resonance imaging was also performed in 5 cases, arthrocentesis and angiography were performed in 1 case. Conservative treatment may include immobilisation, ice therapy, compression or deep tissue massage. Surgical treatment was used in 5 cases. There complete excision of the hemangioma and hemostasis of associated blood vessels is recommended with complete pathology and histologic work-up of the mass. Alternatively, the patient may elect to attempt sclerosing injections or endovascular embolisation.

Conclusions.

1. Intramuscular hemangiomas are rare, more common in children and adolescents, and it is important to differentiate them from other diseases.
2. The lower extremity, especially the thigh as it was observed is commonly involved.
3. Skeletal muscle hemangiomas are completely treatable, and the knowledge of their natural history, clinical findings and imaging appearances are of great importance for proper diagnosis and treatment.

Evaluation of Foot Medial Longitudinal Arch Deformities Using the Calcaneal Inclination Angle

Veronika Boikova, Faculty of Medicine, 4th year
Supervisor – *Dr. med.*, Associate Professor Dzintra Kažoka

Introduction. The longitudinal arch of the foot, composed of medial and lateral parts, acts as a unit with the transverse arch, spreading the weight in all directions. Although there is still no consensus for medial longitudinal arch (MLA) measurement in orthopaedics, there are several suggested radiographic parameters one of which is calcaneal inclination angle or also called calcaneal pitch angle (*Ohuchi et al.*, 2019). It is an angle formed by a line tangent to the inferior cortex of the calcaneus and a horizontal reference line or the plantar plane (*Saraiva et al.*, 2015). The alignment of the hindfoot is determined by this angle. It increases in *cavus* deformity and decreases in flatfoot (*Yalcin et al.*, 2010).

Aim. The aim of the study was to evaluate the MLA of 17 dry feet samples using the calcaneal inclination angle and compare findings with literature provided parameters for diagnostics of medial longitudinal arch deformities such as *pes planus* and *pes cavus*.

Materials and Methods. To evaluate the MLA the calcaneal inclination angle (CIA) was used. It was detected on photographs of 8 left and 9 right dry feet samples from the materials that were provided by Laboratory of Anatomy of the Department of Morphology of the Institute of Anatomy and Anthropology, Rīga Stradiņš University. CIA was measured digitally using the computer program “*Angle Meter 360*”. Descriptive analysis of CIA measurements was made separately for right and left feet samples and was presented by mean value, standard deviation (SD), standard error of the mean (SEM) and confidence interval of the mean (CI). All measurements were taken and analysed based on the technique and criteria described by *Saraiva et al.* at European Society of Musculoskeletal Radiology (ESSR) Congress in 2015.

Results. The mean values of the CIA described in literature are as follows: normal range: 20.0 – 30.0°; flatfoot (*pes planus*): < 20.0°; *pes cavus*: > 30.0° (*Saraiva et al.*, 2015). The finding of the research showed mean value of left feet CIA to be 23.8° (95% CI 16.7° to 30.9°) with modal value – 13.0° and right feet CIA was 20.8° (95% CI 16.3° to 25.3°) with modal value – 26.0°. From provided 17 dry feet samples 4 right feet and 1 left foot CIA showed to be normal (20.0°–30.0°), 4 right feet and 4 left feet CIA appeared to be decreased (< 20.0°) with minimal values between right feet samples – 12.0° and left feet samples – 13.0°, which

indicated presence of flatfoot (*pes planus*) and 1 right foot and 3 left feet CIA was increased ($> 30.0^\circ$) with maximal values between right feet samples – 32.0° and left feet samples – 38.0° , which indicated presence of *pes cavus*.

Conclusions.

1. The medial longitudinal arch is one of the major components affecting foot functions.
2. Results of the research show that the more common detected MLA deformity using calcaneal inclination angle (CIA) occurred to be flatfoot (*pes planus*) in 8 samples and the less common deformity was *pes cavus*, which was detected in 4 samples.
3. In the alignment of the hindfoot 5 samples showed no abnormalities.
4. Medial longitudinal arch deformities can present asymptomatic but also can result in pain, difficulties walking and performing physical activities as well as other complications.
5. Further research is needed for selecting the most appropriate clinical and radiographic diagnostic methods in order to provide accurate screening protocol of medial longitudinal arch deformities.

Illustration of FIGO Classification of Uterine Fibroids

Elisa Bozzotto, Faculty of Medicine, 3rd year
Supervisor – *Dr. med.*, Associate Professor Dzintra Kažoka

Introduction. Uterine leiomyomas or fibroids are the most common benign pelvic tumours in women of reproductive age and affect 20–40% of those women (*Khan et al.*, 2014). 75% of them are found in hysterectomy specimens (*Unkels*, 2012). They are often discovered incidentally in the imaging process for other reasons.

Depending on fibroids size and location, according to the International Federation of Gynecology and Obstetrics classification (*FIGO PALM COEIN* method), it is possible to divide them in three macro groups: submucosal, intra-mural and subserosal (*Laughlin-Tommaso et al.*, 2017).

Aims. The aims of this study were to focus on the gross and macroscopically appearance of the fibrinoids in the uterus and to classify them using the 2011 International Federation of Gynecology and Obstetrics (FIGO) staging system.

Materials and Methods. Materials provided by the Laboratory of Anatomy of the Department of Morphology at the Institute of Anatomy and Anthropology were used. During the dissection procedure out of the 8 available uterus fibroids with different dimensions and localisation were presented in 7 uteri. All fibrinoids were classified into 8 numbers, where the 1st and 2nd belong to the same uterus where two different fibroids were identified. From the 3rd fibroid till the 8th each one of them belongs to a different and separated uterus. After this division, each of the fibrinoids was related to the corresponding number of the FIGO system of 8 different categories. Each fibroid was measured with a digital ruler and sizes were expressed in cm.

Results. The 1st examined fibrinoid can be classified as subserosal pedunculated which corresponds to number 7 of the FIGO system and a dimension of 0.4 cm. Also, the 4th found fibrinoids can be possibly classified as subserosal pedunculated but there the cavitation was observed with a diameter of 0.7 cm.

The 2nd and 3rd fibrinoids examined could be classified as subserosal with at least > 50 % of its surfaces in the intramural region, which correspond to number 5 of FIGO classification and a diameter of 0.6 cm and 2.0 cm, respectively.

The 5th and 8th specimen are described as 100 % intramural with a diameter of 1.0 cm and 3.0 cm and the corresponding number 4 of the FIGO classification.

The 6th specimen can be described both as submucosal with at least < 50 % of its surface intramural or even with more than 50 % of its surface intramural. It was difficult to even macroscopically determine if this fibrinoid belonged to the 1st or 2nd FIGO classification. The size of the examined structure was 2.5 cm in its longest part.

The 7th specimen was classified as subserosal with < 50 % of its surface located intramurally which correspond to FIGO number 6 and with a dimension of 0.7 cm.

Conclusions.

1. Different classifications of fibroids can be found in the literature.
2. Fibroids can range in number from single to multiple and size from very small to large.
3. It was possible to detect more than one type of fibroids and their location in this study.
4. The current FIGO classification showed a lot of limitations during the clinical application.
5. Artificial Intelligence (AI) algorithms to diagnose and classify the fibroids can lead to more accuracy in the classification, therefore implementing the treatment outcome for the patient.

Celiac Plexus and Its Block: Anatomical Review, Indications and Comparison of Techniques

Liena Gasīņa, Faculty of Medicine, 2nd year
Supervisor – *Dr. med.*, Associate Professor Dzintra Kažoka

Introduction. The celiac plexus (*plexus coeliacus s. solaris*) is a large network of sympathetic and parasympathetic nerve fibers surrounding the celiac axis at the T12 – L2 vertebral levels. The greater and lesser splanchnic nerves supply the sympathetic contribution to the celiac plexus. The parasympathetic contribution consists of a small contribution from the anterior vagal trunk and a larger contribution from the posterior vagal trunk (*Candal et al., 2020*). The visceral pain transmitted by the celiac plexus is related to the pancreas, diaphragm, stomach, liver, spleen, small bowel, transverse colon, suprarenal glands, kidneys, abdominal aorta and mesentery (*Pereira et al., 2014*).

A celiac plexus block (CPB) is an injection of local anaesthetic or other medication around the nerves. The CPB technique was first described by *Kappis et al.* in 1919. As image guidance started becoming widespread, *Jones* in 1957 described the use of ethanol-induced celiac plexus neurolysis for long term pain relief. This method is now well-established. The major indications for this medical procedure are abdominal pain and it is prescribed mostly in cases of upper abdomen cancer, chronic pancreatitis, metastases, painful retroperitoneal tumors and chronic abdominal pain in patients who do not respond to treatment, based on high-dose narcotic analgesia. Several approaches have been described to perform the CPB (*John et al., 2020*).

Aims. The aims of the study were: to learn the anatomy of the celiac plexus and determine possible variabilities from theoretical sources; to describe and compare possible celiac plexus block methods, define the advantages and disadvantages; to find out and describe the situation about using CPB methods in Latvia.

Materials and Methods. Different sources (Anatomy atlases, books, medical studies from databases such as *PubMed, ScienceDirect, NCBI*) were used as theoretical background. Data and statistics were taken from the *World Health Organisation, Disease Prevention and Control Center, Health statistics Database, Globocan 2020, Journal of Pain and Symptom Management*.

Results. CPB can be made mostly in 3 ways: percutaneously, surgically or under endoscopic ultrasonography (EUS) guidance. The most described and studied method is a percutaneous approach, which is divided into sub-methods, most used are posterior and anterior para-aortic approaches (*John et al., 2020*). In the anterior approach, a needle is inserted through the anterior abdominal wall,

crossing the abdominal structures, directly into the region of the celiac plexus, and the neurolytic agent is injected into the antecrural space. In the posterior approach, a needle is inserted through the paraspinous musculature into the region of the celiac plexus and a neurolytic agent injected into the antecrural space. Other less common approaches include transaortic and trans-intervertebral disc (*Nitschke and Ray, 2013*). Surgical CPB can be performed during laparotomy or laparoscopy, although newer techniques have largely replaced surgery for performing celiac plexus block. The needle is pierced through the stomach wall and then the medicine is injected into the celiac plexus.

The role of CPB in the pancreas and chronic pancreatitis is best described in the reviewed medical studies (*Gress et al., 2020*). The most reported adverse events include local pain, diarrhoea and orthostatic hypotension. Paraplegia, leg weakness, sensory deficits, and paresthesia, and others have rarely been reported.

In Latvia, the incidence of cancers associated with possible CPB is around 22% of all new cancer cases in 2020 (*Globocan 2020*).

Conclusions.

1. CPB is a long-term result and minimally invasive method that is useful in the diagnosis and treatment of upper abdominal pain.
2. In CPB the nerve fibers responsible for pain transmission are blocked, thus allowing for a possible pain reduction.
3. This procedure is an important tool in the management of patients with abdominal malignancy in whom the pain is not responsive to oral narcotics or who develop important side effects to these.

Architecture of Heart Valve Vegetation in Infective Endocarditis Patients Examined Using Transmission Electron Microscopy

Niks Ričards Goldiņš, Faculty of Medicine, 4th year
Supervisors – *Dr. habil. med.*, Professor Valērija Groma¹;
*Dr. Kristiāns Meidrops*²

¹ Rīga Stradiņš University, Institute of Anatomy and Anthropology, Latvia

² Pauls Stradiņš Clinical University Hospital, Latvia

Introduction. In patients with infective endocarditis (IE), vegetations can develop on any type of heart valves, even though on mechanic and bioprosthetic valves. The major cause of vegetation formation is injured endothelium of the endocardium when destructive structures become adhesive to platelets, immune system cells, and microorganisms. Some of the vegetations are acellular masses, others contain blood platelets, neutrophils, eosinophils, macrophages, erythrocytes and giant cells. In septic patients, sterile platelet-fibrin nidus become secondarily infected. The most common microorganisms supporting the vegetation are *Streptococcus* species, *Bartonella*, and *Staphylococcus* species. To better understand vegetation growth and viability of microorganisms displayed despite the exposure to antibacterial therapy, the study aimed to analyse vegetation ultrastructure by transmission electron microscopy (TEM).

Aim. The aim of the study was to examine the architecture of the heart valve vegetation in IE patients using TEM.

Materials and Methods. Vegetation materials were collected during valve replacement surgery, fixed in 2.5% glutaraldehyde in 0.1 M phosphate buffer, postfixed in OsO₄, dehydrated in ethanol and acetone, embedded in epoxy resin. Ultrathin sections were cut with ultramicrotome, collected on copper mesh grids, and stained with uranyl acetate and lead citrate. The sections were examined in a JOEL 1011 transmission electron microscope at 3000–30,000 magnification. Seven IE patients' vegetations were examined.

Results. More than one vegetation attached to the valve leaflet was detected. In two samples among seven, microorganisms were demonstrated. Blood platelets, neutrophils, macrophages, and other cell types were found. The cellular density varied from highly packed and intermixed cells to a single cell trapped in an extracellular matrix. Additionally, high-density fibrin regions, extracellular vesicles, pseudomyelin figures, collagen microfibrils, and other structures were found; being more organised in the vicinity of fibroblasts. Often, intracellular and extracellular lipid inclusions were demonstrated.

Conclusions.

Ultrastructurally, the appearance of vegetation varies. Neutrophils are present in most vegetations.

Frequently Reported Drugs: Inducers of the Phototoxicity

Arta Grabčika, Faculty of Pharmacy, 4th year
Supervisor – *Dr. med.*, Associate Professor Dzintra Kažoka

Introduction. Drug-induced photosensitivity refers to the development of cutaneous manifestations as a result of the combined effects of chemicals and light. Exposure to chemicals or only light is not sufficient to induce disease. However, photoactivation occurs when chemicals may occur in one or more events. Photosensitivity reactions may result from topical and systemic drug administration wavelengths of ultraviolet A range, so that particular product is more likely to cause induced photosensitivity reactions. However, occasionally ultraviolet B may be responsible for such effects (*Moore et al.*, 2002).

Aim. The aim of this study was to collect information about frequently reported drugs with phototoxicity.

Materials and Methods. Studies from different pharmacology books and medical information from *PubMed*, *AccessMedicine* and other sources were analysed. Only English-language publications were reviewed.

Results. Numerous drugs have the potential to cause phototoxicity. Clinical symptoms vary from light sunburn-like sensation (burning, erythema) to large-area photodermatitis. Most compounds are activated by UV-A, although some have a maximum absorption in ultraviolet B's visible range. The compound's photoactivation determines the excitation of electrons in a stable form in one excited. As the electrons are returning to a more stable configuration, they transfer their energy oxygen leading to the formation of reactive oxygen intermediates (*Lugović et al.*, 2007).

Travellers to tropical countries taking doxycycline for malaria prophylaxis need thorough medical counselling to avoid possibly severe phototoxic reactions (*Goetze et al.*, 2017). Tetracyclines (demeclocycline and doxycycline) can act as light-activated antibiotics by binding to bacterial cells and killing them only upon illumination (*Hamblin et al.*, 2019).

Phototoxic reactions are the most common dermatological adverse effect of amiodarone therapy, affecting 25–75% of patients on long-term treatment. The reaction mechanism seems to be connected with the creation of active metabolites due to radiation, such as oxygen-free radicals. Prevention of acute reactions caused by sunlight in patients treated with amiodarone should include avoidance of frequent sun exposure on the skin and the proper application of external sun protection products with high protection factors (SPF 50 or 50+), reapplied not less frequently than approximately every 2 hours (*Jaworski et al.*, 2014).

Wheal-and-flare reactions following exposure to ultraviolet radiation, were demonstrated following naproxen and nabumetone administration that are nonsteroidal anti-inflammatory drugs (*Kaidbey et al.*, 1989).

Adverse cutaneous reactions occur most frequently with benoxaprofen, piroxicam, sulindac, meclofenamate sodium, zomepirac sodium, and phenylbutazone. The most severe adverse cutaneous reactions, Stevens-Johnson syndrome and toxic epidermal necrolysis, appear to be most often associated with sulindac and phenylbutazone. Among the currently marketed nonsteroidal anti-inflammatory drugs, piroxicam seems to have the highest rate of phototoxic reactions (*Bigby et al.*, 1985).

There is an increasing recognition that long-term voriconazole use is associated with accelerated sun-induced skin changes that include acute phototoxicity reactions, photoaging, actinic keratosis and, especially among immunocompromised patients, skin cancers (*Goyal et al.*, 2015).

Conclusions.

1. Phototoxicity has been attributed to numerous drugs.
2. The most frequently reported drugs were tetracyclines (demeclocycline and doxycycline), amiodarone and nonsteroidal anti-inflammatory drugs.
3. Voriconazole prescription must be associated with strict photoprotection.
4. More scientific studies would be helpful to better predict drug photosensitivity, manage cutaneous adverse events and find the most appropriate alternative treatment strategy.

Anatomical Variation of the Greater Palatine Foramen in a Digital Cranium Collection

Frederik Kipp, Faculty of Medicine, 5th year

Supervisor – *Dr. med.*, Associate Professor Dzintra Kažoka

Introduction. The greater palatine foramen (GPF) can be found at both the left and right posterior angle of the hard palate. It contains the descending palatine artery, the 3rd branch of the maxillary artery, as well as the greater and lesser palatine nerve, both of which are branches of the 2nd cranial nerve.

A nerve block of both the greater and lesser palatine nerve may be used in dental procedures to induce anesthesia in the hemimaxilla. According to *Georges et al.* (2015), the palatine nerve block has lost popularity due to various complications including diplopia and ptosis among others. He states that the complications are likely caused by improper technique and insufficient knowledge of the morphology of the greater palatine foramen. There are varying opinions about the location of the greater palatine foramen in most of the books (*Singh et al.*, 2019).

Aim. The aim of the study was to detect the variations of the greater palatine foramen in 15 crania from a digital cranium collection and to provide further knowledge concerning the anatomical variation of the GPF.

Materials and Methods. Due to the situation caused by Covid-19 pandemic, measurements are taken on photopictures of the skulls with the help of *Gimp*. Pictures of the first nine skulls were provided by the Laboratory of Anatomy of Department of Morphology at the Institute of Anatomy and Anthropology. Six further skull pictures were taken from a *Google* free available images search.

Based on a study conducted by *Ortug* and *Uzel* in 2018, the following measurements have been taken: Palatal Index (PI) and the distance of GPF to the sagittal plane, posterior nasal spine and incisive foramen. Range of the lesser palatine foramina (LPF) was also detected. For all the values measured, the mean and the standard deviation were calculated individually for right and left sides. The findings were tabulated and analysed statistically, using SPSS.

Results. Mean measurements of the GPF are: distance to sagittal plane on the left side 24.08 ± 6.69 mm, on the right side 25.36 ± 7.45 mm; distance to incisive foramen on the left side 58.94 ± 20.85 mm, on the right side 58.85 ± 21.30 mm; distance to the posterior nasal spine on the left side 26.42 ± 7.61 mm, on the right side 27.79 ± 8.43 mm. Based on the PI, three groups can be distinguished – leptostaphyline: $PI < 80$ (1 skull); mesostaphyline: $80 < PI < 85$ (4 skulls) and brachystaphyline $85 < PI$ (10 skulls).

All skulls had a singular GPF on each side. In some skulls the opening of the GPF was obscured by folds in the hard palate. The form and shape of the GPF varied. This might be explained by loss of and breaks in bone structure. LPF showed a greater variance. They were absent in 2, singular in 9 and multiple in 4 skulls. One skull showed a singular LPF on the right side, while no LPF was found on the left side.

Conclusions.

1. All obtained measurements showed a high range of variations of GPF between sides, and these results can be compared to the results of other authors.
2. Differences in distances of GPF to the sagittal plane and to posterior nasal spine were found in this study.
3. The morphometric knowledge about the anatomical position of the greater palatine foramen can be utilized for greater palatine nerve block and surgical procedures in hard palate, anthropological studies and classification of crania.

Pubic Arch Angle as a Predictive Factor of Childbirth Outcome

Krista Koliste, Veronika Boikova, Faculty of Medicine, 4th year
Supervisor – *Dr. med.*, Associate Professor Dzintra Kažoka

Introduction. Every day, millions of women give birth all around the world. It is really important to provide the best possible care for them. Assessment of pelvic configuration is an important factor in the prediction of a successful vaginal birth (*Perlman et al.*, 2019). The pubic arch represents the anterior triangle of the pelvic outlet, formed by the interischial tuberosity diameter as the base and the inferior pubic rami as the sides. The angle at the point at which they converge is known as the pubic arch angle or PAA (*Gilboa et al.*, 2013). This angle provides indirect information about obstetric dimensions that can help to predict possible childbirth outcomes.

Aim. The aim of the study was to measure pubic arch angle of seven female pelvis samples and associate variations of widths of pubic arch angle with different outcomes of childbirth described in the literature.

Materials and Methods. The pubic arch angles were detected on seven female pelvis samples provided by the Laboratory of Anatomy of the Department

of Morphology of the Institute of Anatomy and Anthropology, Rīga Stradiņš University. Measurements of the angle between the left and the right inferior pubic rami were made digitally using computer program “*Angle Meter 360*”. Descriptive analysis of pubic arch angle measurements was made and was presented by mean value and standard deviation (SD). Obtained data was compared with potential outcomes of childbirth depending on width of pubic arch angle described in literature.

Results. The finding showed that the mean pubic arch angle was $99^\circ (\pm 9.3)$, range $88-115^\circ$). Two of the samples had the pubic arch angle wider than 100° , accordingly 115° and 108° . The narrowest PAA were 88° . *Gilboa et al.*, 2013 suggest that the predicted probability for operative delivery increases from 24 % for PAA of 135° to 93 % for a PAA of 80° . The possible reason for higher risk can be explained with the unsuccessful internal rotation of foetus during second stage of labour because of obstruction due to narrow pubic arch angle, which can lead to prolongation of this stage and result in operative delivery. Another risk that is associated with narrow pubic arch is an increased likelihood of occipito-posterior position of foetus which potentially can cause prolongation of second stage of labour, higher incidence of instrumental delivery and, consequently, postpartum anal sphincter trauma and incontinence.

Conclusions.

1. Applying the knowledge acquired from results of *Gilboa et al.*, 2013 prospective cohort study, it can be concluded that in the current study with mean PAA value of 99° the probability of operative delivery could potentially be up to 80%.
2. Pubic arch angle measurement before labour is helpful in predicting the risk of operative delivery. The probability of operative delivery decreases with wider pubic arch angle and increases with narrow PAA.
3. Further research is needed to gain more understanding of PAA importance as predictive factor of labour outcome in order to provide the most suitable care for women before and during childbirth.

Local Defence System in Healthy Lungs

Elizabeta Lohova, Faculty of Medicine, 4th year
Supervisor - *Dr. habil. med.*, Professor Māra Pilmane

Aim. Respiratory system is one of the main infection entrance gates. The aim of this work was to compare specific mucosal pro-inflammatory and common anti-microbial defence mediator activities in different health lung tissue.

Materials and Methods. Healthy lung tissues were collected from 15 patients (3 females and 12 males) in the age from 18 to 86. Immunohistochemistry to HBD-2, HBD-3, HBD-4, LL-37 and IL-17A were proceeded.

Results. Few to moderate HBD-2 positive structures was observed in alveolar epithelium, with strong positive correlation to LL-37 in glands ($\rho = 0.840$, $p < 0.001$), HBD-3 in alveolar epithelium ($\rho = 0.744$, $p = 0.004$), HBD-3 in alveolar macrophages ($\rho = 0.739$, $p = 0.004$). Statistically significant difference was found in alveolar epithelium between HBD-2 and IL-17A ($p = 0.032$). Moderate positive cells of HBD-2 were observed in hyaline cartilage and showed strong positive correlation with IL-17A in glands ($\rho = 0.705$, $p = 0.003$). Statistically significant difference was found between HBD-2 in cartilage and HBD-3 (0.006), HBD-4 ($p = 0.008$). Few HBD-2 positive structures in bronchial epithelium demonstrated significantly strong difference with LL-37 ($p = 0.038$), IL-17A ($p = 0.017$). Strong positive correlation between HBD-2 in bronchial epithelium and HBD-4 in bronchial epithelium ($\rho = 0.740$, $p = 0.009$). Distribution of HBD-2 in glands showed occasional number of immunoreactive cells. There were observed few positive structures in connective tissue and few to moderate positive structures in alveolar epithelium.

Moderate HBD-3-positive structures in alveolar epithelium demonstrated strong positive correlation with HBD-3 in alveolar macrophages ($\rho = 0.857$, $p < 0.001$), LL-37 in glands ($\rho = 0.756$, $p = 0.003$). Statistically significant difference was detected between HBD-3 and IL-17A in alveolar epithelium ($p = 0.034$). Few immunoreactive cells of HBD-3 in bronchial epithelium demonstrated strong positive correlation with HBD-4 in alveolar epithelium ($\rho = 0.791$, $p = 0.011$). Statistically significant difference was found in bronchial epithelium between HBD-3 and LL-37 ($p = 0.038$), HBD-4 ($p = 0.038$), IL-17A ($p = 0.016$). Few HBD-3 positive cells in glands demonstrated strong positive correlation with HBD-4 in bronchial epithelium ($\rho = 0.721$, $p = 0.012$ and also HBD-3 in glands showed similarity with HBD-4 ($p = 0.015$). The HBD-3-containing alveolar macrophages range from few to moderate, with strong positive correlation to LL-37 in glands ($\rho = 0.782$, $p = 0.002$). Distribution of HBD-3 in alveolar macrophages fluctuated

from a few to moderate with statistically significant difference to LL-37 ($p = 0.019$) and IL-17A ($p = 0.008$).

Occasional HBD-4 positive cells in glands demonstrated strong positive correlation with HBD-4 in bronchial epithelium ($\rho = 0.865$, $p = 0.001$). Moderate HBD-4-contained cells in cartilage showed statistically significant difference with IL-17A ($p = 0.004$). Occasional number of HBD-4 positive structures in bronchial epithelium demonstrated statistically significant difference with LL-37 ($p = 0.026$), IL-17A ($p = 0.011$), and such was detected also in glands between HBD-4 and IL-17A ($p = 0.003$), in alveolar epithelium between HBD-4 and LL-37 ($p = 0.043$), IL-17A ($p = 0.026$).

Distribution of LL-37 in bronchial epithelium fluctuated from few to moderate positive cells, with statistically strong positive correlation to IL-17A ($\rho = 0.853$, $p = 0.003$). Statistically significant difference was observed in cartilage between LL-37 and IL-17A ($p = 0.002$), and in bronchial epithelium between LL-37 and IL-17A ($p = 0.025$).

IL-17A immunoreactive structures distribution was observed from occasional in connective tissue to moderate to numerous in cartilage. Bronchial epithelium, alveolar epithelium and alveolar macrophages demonstrated moderate number of positive IL-17A structures, but in glands there were detected only a few positive cells.

Conclusions.

1. Interrelated changes of HBD-3 and HBD-4 expression in different tissue confirms synergistical cooperation of these two mediators in the lung host defence.
2. Significant detection of HBD-2 in healthy lung cartilage showed functional plasticity of the hyaline cartilage including antimicrobial activity and HBD-2 involvement in anti-inflammatory processes of the cartilage.
3. Possible involvement of LL-37 and IL-17A in cartilage immune processes was showed by increased levels of mediators.

Anatomical Variants of the Internal Jugular Vein and Its Importance in Vascular Access for Catheterisation

Angelina Makarova, Egija Junusova, Faculty of Medicine, 4th year
Supervisor – *Dr. med.*, Associate Professor Dzintra Kažoka

Introduction. Catheterisation of peripheral and central veins is one of the most common procedures in medical practice. It is important to have a clear understanding of the anatomy of the internal jugular vein (IJV) and its relationship to the other arteries and veins. This vein is often chosen for its reliable anatomy, accessibility, low complication rates, and the ability to employ ultrasound guidance during the procedure. At the root of the neck the right IJV is placed at a little distance from the common carotid artery (CCA), and crosses the first part of the subclavian artery. The right vein is generally larger than the left, and each contains a pair of valves, which are placed about 2.5 cm above the termination of the vessel.

Aim. The aim of this study was to explore anatomical variants of the IJV with regard to the diameter of the veins lumen and to define their clinical importance in vascular access for catheterisation.

Materials and Methods. Different data bases *NCBI, PubMed, UpToDate*, anatomical books, applications and sources were used for analysis of the variants of the IJV, course, topography and understanding of the catheterisation technique. 3 dominant (anterolateral, anterior, then lateral) variants were described and analysed.

Results. IJV is the largest vein of the neck. It begins on the outer base of the skull in the region of the jugular foramen. On the neck, it is part of the neurovascular bundle of the neck, located lateral to the CCA and vagus nerve. The vein ends at the bottom of the lower bulb, which is located in front of the fusion of the IJV with the subclavian vein, as a result of which the brachiocephalic vein is formed. On its way in the neck, the IJV is covered by *m. sternocleidomastoideus* and *m. omohyoideus*.

The position of IJV described as anterolateral, lateral, anterior, medial and posterior. The most common position of IJV in relation to common carotid artery is anterolateral in approximately 80% on both sides (*Raghavendra Prasad*, 2014). In approximately 15% on both sides was found unsafe position of IJV (*Raghavendra Prasad*, 2014). In study by *Lorchirachoonku* (2012), mean transverse diameter of IJV was about 13.0 mm on the right side and 11.0 mm on the left side of the neck.

IJV vein was considered as small when the diameter was ≤ 7.0 mm and was found in approximately 2% on the right side and 4% on the left side. Lateral and anterolateral positions of IJV in relation to CCA were considered as secure positions and the rest of other positions were considered as anatomical variations and dangerous positions (*Raghavendra Prasad, 2014*).

Most common methods that are used to access IJV are landmark-guided technique and ultrasound-guided technique (*Mendenhall, 2021*). It is imperative to identify the anatomic structures before puncturing the IJV of the specific patient to avoid complications.

Conclusions.

1. Anatomical variations of the IJV exist, and all of them become clinically significant in cases where venous access for catheterisation is important.
2. The most frequent position of IJV in relation to CCA was anterolateral followed by anterior, then lateral.
3. Medial and posterior positions of IJV in relation to CCA were considered as dangerous positions.
4. Use ultrasound for puncture and catheterisation IJV in real time when possible for vein identification, enhancement of the likelihood of catheterisation on the first try, and reduce the likelihood of damage to the carotid artery.

Anatomical Aspects of Topography and Clinical Significance of the Carpal Tunnel

Patricia Melike Lucia Mardin, Luīze Līva Striķe,

Faculty of Medicine, 2nd year

Supervisor – *Dr. med.*, Associate Professor Liāna Pļaviņa

Introduction. The carpal tunnel is a unique structure located in the wrist's anterior side that contains nine tendons and one nerve (median nerve). These structures are all together superficially covered by flexor retinaculum, and inferior border is made of carpal bones. From these nine tendons of carpal tunnel, four belong to *m. flexor digitorum profundus*, the other four belong to *m. flexor digitorum superficialis*. One tendon belongs to *m. flexor pollicis longus*. These muscles provide flexion of the thumb and second to fourth fingers. The median nerve arises as a branch from lateral and medial cords of brachial plexus, extending in

the length of the whole arm, where in the wrist area it passes through the carpal tunnel (Reuter, 2019; Rotman and Donovan, 2002). Median nerve, its topography and knowledge about wrist area are crucial regarding identification of the nerve block in carpal tunnel that may lead to carpal tunnel syndrome (Nora et al, 2005). This is particularly significant due to the high prevalence across the whole world of Carpal Tunnel Syndrome (Andersen et al, 2003; Shiri, 2016; Bilge, 2017). Particularly in the United States, the incidence is 9.2% for women and 6% in men, but compared to the United Kingdom, this prevalence is significantly higher. The occurrence for people in the age group from 15 to 65 is very high – 16% (Genova, 2020).

Aims. The aims of the study are: to review and analyse the available literature about the topography of carpal tunnel, clinical significance carpal tunnel syndrome and the median nerve block; to dissect the median nerve and to examine topography of carpal tunnel components.

Materials and Methods. For this dissection project human cadaver was supplied, as well as the equipment used for dissection, by the Laboratory of Anatomy of the Department of Morphology of the Institute of Anatomy and Anthropology.

Results. Analysis of literature sources showed that carpal tunnel is anatomically unique structure. It has very narrow characteristics in which nine tendons for flexor functions and one very important nerve – the median nerve. Median nerve is a mixed nerve providing both motor and sensory fibers. *N. medianus* supplies the palmar side of the thumb, index finger, middle finger and partially the ring finger. Due to carpal tunnel's narrow characteristics, there is a possibility that median nerve can become irritated or compressed, leading to nerve's partial or complete blockage. It would cause paresthesia and possible loss of the motor functions (Nora et al, 2005).

Conclusions.

1. The carpal tunnel syndrome is a common irritation, and it is connected to inappropriate wrist position during work with computer, as well it accompanied such diseases as diabetes mellitus or arthritis.
2. The topographical aspects of carpal tunnel are essential for assessment of the clinical findings: topography and location of median nerve, its course and relationship with tendons of muscles in carpal canal are associated with pathologic changes and disorders in innervation of the skin and muscles of the wrist.

Comparison of Three Types of Central Venous Catheterisation Places

Jekaterina Muravjova, Anastasija Semjonova,

Faculty of Medicine, 2nd year

Supervisor – *Dr. med.*, Associate Professor Dzintra Kažoka

Introduction. Central venous catheterisation was first performed in 1929 (*Smith et al.*, 2013). Since then, central venous access has become a mainstay of modern clinical practice. It is an indispensable procedure in various situations in the intensive care unit, emergency room and operation room. There are many applications such as invasive hemodynamic monitoring, parenteral nutrition support, dialysis, chemotherapy, fluid resuscitation and drug administration, though there are some complications associated with catheter placement – venous air embolism, pneumothorax, vascular perforation, catheter-related bloodstream infections, occlusion, displacement.

Aims. The aims of the study were to compare the central venous catheterisation places theoretically, to analyse techniques, risk factors and complications that might occur, finding the safest and most beneficial venous access.

Materials and Methods. Various books, free internet resources and databases (*ClinicalKey*, *AccessMedicine*, *DynaMed Plus*) were analysed to explore the comparative analysis of central venous catheterisation.

Results. A central venous catheter, also known as a central line or CVC, is a long, soft, thin and hollow tube with a tip that lies within the proximal third of the superior vena cava, the right atrium, or the inferior vena cava. Catheters can be inserted through a peripheral vein or a proximal central vein, most commonly the internal jugular, subclavian or femoral vein. It differs from an intravenous (IV) catheter placed in the hand or arm (also called a “peripheral IV”).

The indications for CVC include access for giving drugs, access to extracorporeal blood circuits, haemodynamic monitoring and interventions. The site of insertion depends on indication for insertion, predicted duration of use, previous line insertion sites and presence of relative contraindications. Incorrect placement of the catheter tip can increase mechanical and thrombotic complications, but the ideal location of the catheter tip depends on the indications for catheterisation and the site of insertion.

Central venous catheters (CVCs) can be inserted through the jugular, subclavian or femoral veins, or via the upper arm peripheral veins (PICC line). The jugular CVC or PICC line are usually preferred to a subclavian CVC that is

associated with a higher risk of bleeding and pneumothorax or femoral CVC that is associated with a higher risk of infection. Three approaches to the internal jugular vein are widely recognised and include central (most commonly used), posterior and anterior approaches. During cardiac arrest, fluid and drugs are given through a femoral vein CVC often fail to circulate above the diaphragm because of the increased intrathoracic pressure generated by cardiopulmonary resuscitation (CPR). In this case, a subclavian or internal jugular approach may be preferred. The subclavian vein is generally cannulated using one of the three anatomic approaches, with a large-bore access needle using landmark techniques. Ultrasound guidance is commonly used and recommended for internal jugular and femoral venous access sites.

Conclusions.

1. Different variants of central venous catheters can be used for the medical procedures.
2. An internal jugular central venous catheter (CVC) or a peripherally inserted central catheter (PICC) is usually preferred to a subclavian CVC or a femoral CVC.
3. Specific veins (jugular, subclavian, femoral) and access approaches have inherent advantages and disadvantages.

Surgical Access to Middle Cerebral Artery in Case of Aneurysm

Roberts Puriņš, Faculty of medicine, 2nd year
Supervisor – *Dr. med.*, Associate Professor Dzintra Kažoka

Introduction. Cerebral aneurysms (CAs) are the common cause of death globally. Statistics show that CAs occurs in 3% to 5% of the general population. Mortality percentage can reach up to 50–60% within the first months (*Steiner*, 2013). 80–85% of nontraumatic subarachnoid haemorrhages (SAH) are associated with CAs. Aneurysm of the middle cerebral artery (MCA) reach 21% of all CAs and is the third incident. It is a structural defect and dilatation of arterial wall with loss of internal elastic lamina and destruction of the media. Risk factors include smoking, hypertension, race, age and gender. Aneurysm rupture occurs when wall tension exceeds the mechanical strength of wall tissue. If the aneurysm is ruptured then it causes SAH.

CAs mostly affect bifurcations, curved vessels (*Chalouhi*, 2013) and can be diagnosed using methods of radiography. Nonsurgical endovascular treatment in case of CAs is coil embolisation and stenting. When nonsurgical methods are not useful, invasive methods such as clipping which require direct access to the artery, are performed.

Aim. The aim of this study was to detect two surgical accesses to MCA using a literature review and to describe possible complications and benefits of these methods in the case of an aneurysm.

Materials and Methods. This review provides an overview of the current literature regarding MCA surgical access and treatment, with the objective to clarify the available evidence of efficiency with surgical compared to nonsurgical treatment. An existing literature search strategy was used with the following terms: *MCA, surgical access and cerebral aneurysm*. The search of articles published between 1984 and 2020 was conducted from the following databases and sources: *Pubmed* and *Brain aneurysm foundation* (BAF).

Results. In the literature, the most mentioned are the two methods, and the use of both of them offers possibilities to access MCA.

The first method to access MCA in case of aneurysm includes 5 steps: positioning, skin incision, craniotomy, dural incision, dissection of Sylvian fissure to expose MCA aneurysm. In positioning the patient is placed in a supine position with the head maintained at 20–40° rotation opposite side of the craniotomy. The backboard was tilted up about 20°. In this method, corkscrew electrodes for transcranial motor-evoked potential (MEP) are placed on both sides of the head. After dissection of sylvian fissure using this method M3 and following M2 segments of MCA are accessible. Further steps, such as a choice between proximal or distal approach, of this method depends on the type of aneurysm, location of it and other factors (*Ikawa*, 2018).

The second method to access MCA in case of aneurysm includes 4 steps: positioning, craniotomy, dural incision, dissection of Sylvian fissure. In positioning the patient is placed in a supine position. The head is fixed in a neutral position with the chin elevated 5–10°. In this method cork screw electrodes for transcranial MEP are not used. After the dissection of Sylvian fissure using this method aneurysms of M1 and M2 segments of MCA will be visible. This method requires dissecting internal carotid artery (ICA) before access of MCA (*Suzuki*, 1984).

Conclusions.

1. Access to MCA is possible in both methods, but there are differences between these methods in position of the head, including corkscrew electrodes, visible segments of MCA and dissection level.
2. The choice between these methods depends on the affected with aneurysm segment of MCA.

Anatomical Macrostructures Related to Development and Expression of Glioblastoma Multiforme (GBM): Literature Review

Daniel Semke, Faculty of Medicine, 2nd year
Supervisor – *Dr. med.*, Associate Professor Dzintra Kažoka

Introduction. The *glioblastoma multiforme* is the most common grade IV WHO malignant primary tumour with astrocyte differentiation. It is characterised by an incurable and aggressive pathological phenotype, which affects typically adults and is more often observed in men than women (*Batash et al.*, 2017). It has an incidence rate of 3.7 per 100 000 person-years and a poor survival rate with a median of 14.6 months after diagnosis (*Poon et al.*, 2020). The main symptoms include headaches, seizures, memory loss, problems with speech, and loss of vision (*Alifieris et al.*, 2015). These latter symptoms could be the result of changes in anatomical macrostructures. There are only a few studies describing the morphology of glioblastoma multiforme.

Aim. The aims of the study were to review the literature and to detect anatomical macrostructures in the brain, which potentially are related to the development and expression of *glioblastoma multiforme*.

Materials and Methods. Several studies and case reports of patients were used for the analysis and comparisons of the findings. The search included a combination of keywords, and the information was detected for the English language studies in the following databases: *Pubmed*, *Sciendirect*, *Nature* and *CaseReports* from December 2016 until August 2018. Different detected tendencies were used to evaluate changes in anatomical structures.

Results. In general, gliomas are located more frequently in the right hemisphere (51%) than in the left (40%) (*Larjavaara et al.*, 2007). There are several morphological changes observed in the brain, which are predominantly found in the frontal and the temporal lobe. When comparing the tumour: volume ratio in the frontal lobe with 4.5 and the temporal lobe with 4.8 (*Larjavaara et al.*, 2007). It indicates that greater tumours are found in the latter. The densest occurrence is located in the anterior subcortical brain. In a study with 267 patients about the anatomic location of gliomas, 68% were located at only one anatomic site, whereas in 32% of the cases the tumour was overlapping over two or more anatomic sites (*Larjavaara et al.*, 2007). The progression of the tumour was observed in the *gyrus precentralis* causing hemiparesis and focal partial seizure (*Jacksonian* seizure). Additionally, the *gyrus angularis* can be affected resulting

in *Gerstmann* syndrome leading to dysgraphia, dyscalculia, finger agnosia and left-right disorientation diagnosis (*Meyer et al.*, 2007). Comparing these pathologically affected *gyri* to healthy reference tissue, it would show lesions causing these neurological deficits thus leaving the morphological structure change as the primary explanation. The tissue to be prone for those lesions can be explained with mechanical differences between healthy glial cells and GBM tumour cells. In comparison, affected cells have lowered cytoskeletal stiffness, cell traction stress and focal adhesion than the healthy cells (*Beliveau et al.*, 2016).

Conclusions.

1. Anatomic and topographic location of a glioma affects treatment options and prognosis.
2. Affected areas in the brain are mainly located in the frontal, temporal and parietal lobes causing several neurological impairments.
3. Causes and mechanisms behind the spreading of glioblastoma multi-forme have not been fully understood, thus further research has to be undertaken.

Evaluation of Different Tissue Factors and Apoptosis in Primary Obstructive Megaureter Tissue

Ivo Siņicins, Faculty of Medicine 4th year
Supervisor – *Dr. habil. med.*, Professor Māra Pilmāne

Introduction. Primary obstructive megaureter (POM) is enlargement of ureter greater than 7 cm in diameter. It has estimated incidence of 0.3 of 1000 newborns and shows yet unknown morphogenesis.

Aim. The aim of the study was to detect appearance and distribution of different factors that participate in regulation, innervation, vascularisation and growth/development of ureters and might take part of pathogenesis in the development of POM.

Materials and Methods. Megaureter tissues of 11 patients (aged from 1 month to 15 years) and 3 children from control group (13 months, 2 and 10 years) were obtained during the surgery. The samples were stained with Haematoxylin and eosin as well as with immunohistochemistry for protein gene product 9,5(PGP9.5), nerve growth factor (NGF), angiotensin 2 receptor type 2 (A2TR2),

matrix metalloproteinase 2 (MMP-2), fibroblast growth factor receptor 1 (FGFR1), transforming growth factor beta 1 (TGF β 1) and sonic hedgehog (SHH). Apoptosis was detected by TUNEL reaction.

Results. POM tissues revealed transitional epithelium with scattered vacuolization, submucosa with patchy inflammatory cells infiltration, focally vacuolized, atrophic, chaotically organized layers of smooth muscle cells and adventitial connective tissue. Neuropeptide-containing innervation, number of NGFR1 A2TR2, SHH did not differ between the patients and controls, while apoptosis, appearance of MMP-2, FGFR1 and SHH prevailed in the patient tissue. Interestingly, TGF β 1 positive cell number was much lower in connective tissue of patients in comparison to the controls. Multiple significant differences between POM affected tissues and controls were revealed: in number of apoptotic epithelial cells ($p = 0.021$), apoptotic smooth muscle cells ($p = 0.046$), MMP-2 epitheliocytes ($p = 0.009$), MMP-2 positive connective tissue cells ($p = 0.007$), MMP-2 positive endotheliocytes ($p = 0.014$), FGFR1 positive epitheliocytes ($p = 0.032$), and SHH positive cells ($p = 0.007$). Very strong positive correlation between MMP-2 in epithelium and endothelium ($r_s = 0.867$, $p = 0.00$), MMP-2 and FGFR1 in epithelium ($r_s = 0.805$, $p = 0.005$), and TGF β in epithelium and connective tissue ($r_s = 0.924$, $p = 0.000$) in patients was detected.

Conclusions.

1. POM morphopathogenesis involves the dynamic apoptotic cells death in epithelium and smooth muscles, and tissue degradation in epithelium, connective tissue and blood vessels of ureter wall.
2. The decrease of tissue growth by diminished TGF β expression with stimulation of renal growth factor receptors FGFR1 suggests the tissue remodellation disbalance in megaureter wall.

Morphological Analysis of Alcohol-induced Destruction in Liver Parenchyma

Marija Skultecka, Faculty of Medicine, 3rd year
Supervisor – Assistant Professor Sandra Skuja

Introduction. Liver is the biggest organ of the digestive system and the only one in the human body that is responsible for alcohol detoxification process. Each acute and chronic ethanol consumption is accompanied by an acceleration of lipogenesis, namely, an increased synthesis of phospholipids and triglycerides, which are made of a glycerol and three fatty acids. An overproduction of fatty acids is hepatotoxic as they are a base for triglycerides production, which lead to the first stage of chronic alcohol disease called steatosis. Steatosis is an accumulation of fat molecules in the hepatocytes' cytoplasm in the form of microvesicles or macrovesicles. It is a reversible stage in case of stopping an abuse of alcohol as liver can regenerate. In turn, steatosis can lead to alcoholic hepatitis, a condition of inflammation in portal regions, which can evolve into liver fibrosis. Subsequent hepatocytes necrosis and regeneration followed by fibrosis results in cirrhosis, which is nodules of hepatocytes fully surrounded by connective tissue septa.

Aim. The aim of the study was to define alcohol-induced morphological changes in liver tissue.

Materials and Methods. 59 autopsy materials were analysed, of which 14 were young alcohol users, 33 were chronic alcohol users (alcoholics) and 9 were from a control group. In H&E slides microvesicular and macrovesicular lipid inclusions (steatosis), ballooned hepatocytes, portal inflammation and fibrosis were evaluated. The lesions found in the liver parenchyma were assessed using semi-quantitative method. The slides were analysed in the light microscope with a 400× magnification. Statistical data analysis was done by GraphPad Prism v.6 programme and SPSS v22.0. Data were presented as medians with interquartile range (IQR (25%; 75 %)).

Results. It was found that 76% of alcoholics had microvesicular steatosis and both control group and young alcohol users were free of it. The research obtained that 55% of alcoholics had macrovesicular steatosis 2.00 (0.00; 3.00), that was negatively correlated with microvesicular steatosis 1.00 (0.00; 2.00), ($r = -0.508$, $p < 0.001$). Also, alcoholics' macrovesicular steatosis was correlated with portal inflammation ($r = 0.179$, $p < 0.001$) and with fibrosis ($r = 0.198$, $p < 0.001$). It was detected that 82% of alcoholics had ballooning 2.00 (1.00; 2.00) that correlated with macrovesicular ($r = 0.658$, $p < 0.001$) and microvesicular steatosis ($r = -0.386$,

$p < 0.001$). The study found that 57% of young alcohol users and 85% of alcoholics had portal inflammation that correlated with fibrosis ($r = 0.343$, $p < 0.001$). The analysis allowed to observe that 82% of alcoholics had fibrosis and 6% of them were in the stage of cirrhosis.

Conclusions.

1. Prolonged alcohol overconsumption can lead to a wide spectrum of liver pathologies ranging from hepatic microvesicular and macrovesicular steatosis to steatohepatitis that evolve into liver fibrosis, cirrhosis.
2. An increased presence of macrovesicular steatosis, ballooning, portal inflammation and fibrosis was found in the case of alcoholics.

Anatomical Aspects of Facial Filler Injection

Jeļizaveta Smirnova, Anna Krauß, Faculty of Medicine, 4th year
Supervisor – *Dr. med.*, Associate Professor Liāna Pļaviņa

Introduction. Knowledge of facial blood supply is crucial for safe administration of dermal fillers in aesthetic medicine where filler injections are used for correction and augmentation of facial features. Incidence of vascular adverse events varies from 1 : 2000 to 1 : 10 000 (*Schelke et al.*, 2020); however, advertising of illegal filler injections by uncertified specialists as well as self-injection techniques are encompassing social media that may lead to unreported complication cases. Cutaneous ischemic necrosis is an uncommon adverse effect of facial filler injection by direct vascular embolisation (*Funt et al.*, 2013) or via vascular compression of arteries supplying skin and mucosa (*Sito et al.*, 2019).

Aim. The aim of the study was to review and analyse the literature about intradermal facial fillers, to dissect the superficial arteries of the face and examine their topographical anatomy in the frontal, orbital, nasal, infraorbital, zygomatic, buccal, oral and mental regions.

Materials and Methods. Laboratory of Anatomy of the Department of Morphology of the Institute of Anatomy and Anthropology has provided the human cadaver and the instruments required for dissection. Theoretical research was performed by literature review.

Results. Analysis of literature has shown that hyaluronic acid and autologous fat were the two fillers most frequently involved in adverse vascular occlusions (*Funt et al.*, 2013). Several arteries can be injured by the needle during filler

injection. Prone areas for tissue necrosis are those which are supplied by one dominant artery without collaterals (*Bravo et al.*, 2015). Regions at increased risk of vascular compromise from compression or embolisation include the frontal region especially the *glabella* via *a. supratrochlearis* and the periorbital region via *a. angularis* and *a. supratrochlearis* (*King et al.*, 2020). The injections in the nasal region in particular the nasolabial folds via *a. angularis*, *a. dorsalis nasi* and *ramus lateralis nasi* of facial artery may cause cutaneous necrosis (*Loh et al.*, 2018) but by retrograde motion and occlusion of *a. centralis retinae* results can end in blindness (*Ozturk et al.*, 2013).

Conclusions.

1. Physicians performing facial filler injections should have a profound knowledge of facial anatomy to perform the procedure, using correct injection techniques in safe facial areas taking into consideration anatomical variations by vascular mapping to avoid possible complications. Serious complications with soft tissue fillers from the accidental intra-arterial injection of filler material may lead to vascular occlusion, cutaneous necrosis or in the most disadvantageous cases blindness or stroke.
2. Facial areas with underlying paths of *a. facialis*, *a. ophthalmica* and their branches have the highest risk of injury, embolisation and further adverse events during filler injection procedures.

Ki-67 and PTEN Expression in Endometrial Hyperplasia and Cancer

Estere Strautmane, Faculty of Medicine, 3rd year
Supervisor – Assistant Professor Sandra Skuja

Introduction. Endometrial hyperplasia (EH) is very common across women, especially after menopause (133 in 100,000 per year). Atypical hyperplasia (AH) is considered as a precursor for endometrial carcinoma (EC) and can develop from EH. Mutations in tumour suppressor protein gene PTEN are the most frequent genetic lesions in endometrial adenocarcinomas. In EC development, a significant emphasis is put on inactivation of PTEN tumour suppressor gene and activation of cycle regulatory protein, proliferation marker Ki-67 therefore, early diagnosis and pathogenetically justified treatment of the disease are the basic conditions for the prevention of EC.

Aim. The study was undertaken to examine the expression of cell cycle regulatory and tumour suppressor proteins in endometrial hyperplasia (simple and atypical) and endometrial carcinoma.

Materials and Methods. Obtained surgical tissue samples from 9 women with endometrial hyperplasia, 6 with atypical endometrial hyperplasia and 9 with endometrial cancer were examined. Immunohistochemical staining for PTEN protein was performed with monoclonal antibody 25H6. Anti-Ki67 monoclonal antibody as proliferation marker was used. In each of the slides 10 visual fields were selected and quantitative counting of all positive cells was done. SPSS Statistics v.23 was used to analyse the data.

Results. Statistically reliable ($p < 0.005$) that in EHs as well as AHs and ECs PTEN expression in the epithelium was more pronounced than Ki-67 expression. A statistically reliable ($p < 0.005$) PTEN expression in the epithelium was more pronounced than Ki-67 expression in EHs as well as AHs and ECs. There was a moderately strong negative correlation in the EHs - the more Ki-67 positive cells were in the stroma, the fewer positive cells in the epithelium ($r = -0.487$, $p = 0.001$). In the ECs there was a moderately strong correlation - the more Ki-67 positive cells were in the epithelium, the more in the stroma ($r = 0.501$, $p = 0.001$). Additionally, a statistically significant correlation ($r = 0.410$, $p = 0.009$) between the Ki-67 positive cells and PTEN positive cells in the stroma were determined.

Conclusions.

Endometrial glandular epithelium cells show more pronounced PTEN than Ki-67 expression in all study groups. In EH cases, more Ki-67-positive cells are observed in the stroma compared to the glandular epithelium, more so, with a negative correlation, which indicates significant changes in the stroma. In the case of EC, this correlation was positive, indicating changes not only in the epithelium, but also in the stroma.

Geometrical Variations of Circle of Willis

Anastasija Ševčenko, Faculty of Medicine, 2nd year

Supervisor – *Dr. med.*, Associate Professor Dzintra Kažoka

Introduction. The circle of Willis is an anastomotic ring of arteries located at the base of the brain connecting the two major arterial systems to the brain. Its main function is to provide an anastomotic connection between the anterior and posterior circulations, providing collateral flow to affected brain regions in the event of arterial incompetency (*Rosner et al.*, 2020). The circle of Willis is a highly variable anatomical complex that may lead to the appearance and severity of symptoms of cerebrovascular disorders (*Iqbal S.*, 2013).

Aim. The study aimed to review and analyse the literature about geometrical variations of the circle of Willis, clinical correlations and cerebrovascular diseases, as well as to compare different variants of the vessels.

Materials and Methods. 30 randomly selected pictures from human cadaveric studies of the brain with a circle of Willis were used in this research. Pictures were accessed free of charge through internet resources. The software programme used to analyse the data was Inkscape. The circle of Willis was analysed with special reference to the following factors – whether the circle is complete or incomplete (aplasia) and a number of the component vessels, duplication or triplication of any of the vessels as well as increase or decrease in the size of the vessels (hypoplasia, hyperplasia). The arteries examined were the anterior communicating artery (ACoA), the proximal and the distal (1 cm) segments of the anterior cerebral (ACA), the internal carotid (ICA) distal to the origin of the posterior communicating (PCoA), middle cerebral (MCA) at its beginning, the posterior communicating, the proximal and distal (1 cm) segments of the posterior cerebral (PCA) and basilar arteries (BA). The results obtained were tabulated.

Results. All the circles of Willis observed were schematised and classified. Out of 30 human cadaveric circles of Willis examined, 20.0% (6) conformed to the typical pattern. The anterior communicating artery was aplastic in 26.67%, duplicated in 10.0% and hypoplastic in 3.34%. The left anterior cerebral artery was duplicated in 3.34% and hypoplastic in 23.34%. The right anterior cerebral artery was aplastic in 6.67%. The left posterior cerebral artery was aplastic in 6.67%, triplicated in 3.34% and hypoplastic in 3.34%. The posterior communicating artery bilaterally was aplastic in 10.0% and hypoplastic in 13.34%. The left posterior communicating artery was aplastic in 3.34% and hypoplastic in 6.67%. The right posterior communicating artery was aplastic in 6.67% and hypoplastic

in 6.67%. The internal carotid artery was hypoplastic in 3.34%. No analysed vessels showed signs of hyperplasia.

Conclusions.

1. Analysis of the literature resources show that the circle of Willis is a network of arteries surrounding the base of the brain, providing collateral circulation to prevent ischemic pathology.
2. In this study the most common anatomic variations were aplasia and duplication of the anterior communicating artery, aplasia of the posterior communicating artery bilaterally and hypoplasia of the left anterior cerebral artery.
3. None of the observed specimens showed hyperplasia of vessels.
4. The patterns and frequencies of variations of the circle of Willis observed in this study will help clinicians and researchers understand the anatomical bases of certain neurovascular diseases.

Access to the Ventral Pontomesencephalic Region of the Brain Through the Different Intracranial Corridors

Laima Unzule, Faculty of Medicine, 2nd year
Supervisor – *Dr. med.*, Associate Professor Dzintra Kažoka

Introduction. The human brain is one of the most complex organs in the human body. There are defined some approaches and triangular corridors in the brain which are used in the neurosurgery to facilitate orientation in the operations. The ventral pontomesencephalic region is technically a difficult region, and many surgical approaches to this area have yet to be perfected. Also the access to this brain area is challenging because of nearby meaningful structures. Understanding the anatomy of the brain intracranial triangles and approaches is very important for approaching surgical lesions. Moreover, the access to the ventrolateral aspect of the pontomesencephalic area and adjacent cisterns is necessary in cases of a variety of pathologies. This could develop new neurosurgical approaches and increase the number of successful neurosurgical operations.

Aims. The aims of this study were to analyse the access to the ventral pontomesencephalic region through different intracranial triangular corridors and to provide an overview of their variations in the clinics and neurosurgery.

Materials and Methods. During this study, the information from different anatomy atlases and research, medical information from *PubMed*, *Clinical Key*, *ResearchGate* databases was taken into consideration.

Results. Two approaches are commonly used for accessing this region: transsylvian and subtemporal. For transsylvian surgical approach, orbitozygomatic craniotomy is used. After the opening of the dura and exposing the sylvian fissure, the carotid, interpeduncular, chiasmatic and crural cisterns can be opened to gain entry to the anterior incisural space. To perform this approach, the venous attachments between the tip of the temporal lobe and the sphenoparietal should be divided. Furthermore, here is also a need to maximize posterior mobilisation of the temporal lobe (*Mascitelli et al., 2018*). After that, the Oculomotor-tentorial triangle (OTT), limited by the oculomotor nerve anteromedially, the medial tentorial edge anterolaterally, the cerebral peduncle posteromedially and the temporal lobe uncus posterolaterally, can be effectively exposed in all specimens (*Tayebi et al., 2018*). After the transsylvian pretemporal approach, where the OTT triangle is reached, there could be two techniques performed to expose triangle and to enlarge ventrolateral pontomesencephalic region. These are transcavernosus approach (TcA) and uncal resection. TcA allows to increase the exposed length of the oculomotor nerve. Resection of the uncus allowed further exposure of the tentorium posteriorly. In subtemporal approach after craniotomy at exposed temporal squama the free edge of the tentorial incisura and the arachnoid sheath of the ambient cistern become visualised. Opening of the cistern will provide further cerebrospinal fluid drainage and clear view of its contents.

Conclusions.

1. Transsylvian and subtemporal approaches are commonly used for ventral pontomesencephalic region.
2. The ability to access the area and the adjacent cisterns is necessary for treating vascular lesions, revascularisation of the upper posterior circulation and for resection of cavernous malformations.
3. Understanding the anatomy of the optico-carotid, supracarotid, carotid-oculomotor intracranial triangles and corridors is very important for approaching surgical lesions, the access to the ventrolateral aspect of the pontomesencephalic area.

Topography and Clinical Importance of Some Intracranial Triangles in the Cavernous Sinus, Middle Fossa and Sellar Region

Laima Unzule, Faculty of Medicine, 2nd year
Supervisor – *Dr. med.*, Associate Professor Dzintra Kažoka

Introduction. In 1960, Parkinson illustrated one of the intracranial triangles, which was located in the lateral wall of the cavernous sinus, and later Dolenc described direct microsurgical approaches in terms of the anatomy and surgery within the corridors of the cavernous sinus (*Drazin, 2017*). In recent years, new triangular corridors have been defined and discovered to access the specific regions of the brain. Therefore, it is very important to describe the topography and clinical importance of these geometric landmarks.

Aims. The aims of this study were to provide an overview of the anatomical borders and surgical implications as well as illustrations of the different intracranial triangles, to describe them and to compare their anatomical features and accessibility, including analysis of their role in the brain surgery.

Materials and Methods. During this study, the information from different anatomy atlases and research, medical information from *PubMed*, *Clinical Key*, *ResearchGate* databases was taken into consideration.

Results. There are four triangles of the cavernous sinus. Dolenc's (anteromedial) triangle is bordered by the optic nerve, oculomotor nerve and tentorial edge. This intracranial triangle is necessary to access to the cavernous internal carotid (ICA) artery (*Granger et al., 2018*). Medial (oculomotor/Hakuba's) triangle is limited by the anterior, posterior and interclinoid dural fold. This triangle can be used for accessing tumours which are situated in the medial cavernous sinus (*Martins et al., 2006*). The paramedian (supratrochlear) triangle's medial border is the oculomotor nerve, and the lateral border is the trochlear nerve. The base is made by the tentorial edge between the third and fourth cranial nerves (*Watanabe et al., 2003*). This triangular window can be used during clipping of cavernous aneurysms. Borders of the infratrochlear (*Parkinson's*) triangle are the trochlear nerve, ophthalmic division and the tentorial edge. This triangle has a role in surgical management of vascular abnormalities along the ICA and also during cranial nerve mass lesions.

Anteromedial (*Mullan's*) triangle is present in the middle fossa. The base of the triangle consists of the anterolateral wall of the bony middle cranial fossa formed by a line connecting the superior orbital fissure to the *foramen rotundum*

(Krayenbuhl, 2007). This corridor is suitable for exposing various necessary structures like orbital vein, sixth cranial nerve, sphenoid sinus and the ophthalmic vein. The borders of anterolateral triangle are the maxillary nerve, mandibular nerve and the *foramen rotundum* to *foramen ovale*. Through this triangle, lesions located in the lateral part of the cavernous sinus can be revealed. The corridor through posteromedial (Kawase's) triangle allows access to the vertebrobasilar junction, the root of the trigeminal nerve and anterolateral brain stem. Posteromedial (Glasscock's) triangle has many variations in the size. This triangle allows to see the horizontal intra-petrosal segment of the ICA for proximal control for a bypass graft or anastomosis, and also allows access to the cavernous sinus for the tumour resection.

In the sellar region are 2 triangles. Parasellar triangle is bordered by the anterior and the posterior petroclinoid dural fold, tentorial edge, the anterior and posterior clinoid process. ICA triangle is used to treat lesions of the sellar region and to access tumours located there (Lieb, 2017).

Conclusions.

1. There are 10 intracranial triangles in the cavernous sinus, middle fossa and sellar region.
2. The corridors made by intracranial triangles allow resecting meningiomas, tumours and play a significant role in the surgical management of the cranial nerve mass lesions.
3. Understanding the anatomy of the brain intracranial triangles is very important for approaching different brain regions and treating various pathologies.

Variations and Clinical Effects of Aortic Coarctations

Paula Marija Vimba, Faculty of Medicine, 2nd year
Supervisor – *Dr. med.*, Associate Professor Dzintra Kažoka

Introduction. Coarctation of the aorta is a heterogenous lesion that generally refers to a congenital narrowing of the thoracic aorta, directly opposite, proximal, or distal to the *ductus arteriosus*, resulting in a pressure gradient (*Nelson et al.*, 2019). However, aortic coarctations can appear throughout the thoracic and abdominal aorta. Coarctation can occur in isolation but is often associated with other congenital heart defects, including bicuspid aortic valve, aortic arch hypoplasia and other arch anomalies, ventricular septal defect, mitral valve abnormalities, subaortic stenosis, among others (*Kim et al.*, 2020). Up to 30% of patients with Turner syndrome also have coarctation of the aorta, and 5% to 15% of girls with coarctation have Turner syndrome (*Alomari et al.*, 2021).

Aim. The aim of this study was to establish in which part of the aorta the narrowings are more common as well as to determine this cardiovascular malformations clinical effect, using images and descriptions from 44 clinical cases, as well as the literature about aortic coarctations.

Materials and Methods. In this study, the practical part was completed using information about symptoms, the course of this congenital disease and photographs of different age groups in 44 patient cases that were accessible in the internet resources (*clinicalkey.com*; *ncbi.nlm.nih.gov*; *pubmed.ncbi.nlm.nih.gov*).

Results. In research studies, two types of coarctations are described – preductal (infantile) and postductal coarctations. Postductal coarctations are categorised by the part of aorta where they appear – thoracic or abdominal aorta. Postductal coarctations are more common in adults, but preductal coarctations are more common in infants. In images from 44 patient cases all types of aortic coarctations were identified – preductal and two types of postductal coarctations. The infantile or preductal aortic coarctation is often associated with major abnormalities. The narrowing is proximal to the *ductus arteriosus* or *lig. arteriosum*. In postductal or adult coarctation, the narrowing is distal to the *ductus arteriosus* or *lig. arteriosum* (*Raeside*, 2009). Middle aortic coarctation or narrowings of the distal thoracic and abdominal aorta are rare anomalies accounting for less than 2% of all aortic coarctations (*Stanley et al.*, 2014).

Symptoms of aortic coarctation depend on the age of discovery as well as the severity of the aortic narrowing, and adequacy of circulation. Neonates with

severe aortic coarctation may present with heart failure and shock when the ductus arteriosus closes. Nevertheless, neonates without severe aortic coarctation may be asymptomatic. After infancy, most patients are asymptomatic. However, symptoms can arise from severe hypertension, which can cause epistaxis, headache, heart failure symptoms and aortic dissection. Claudication of the lower extremities can also occur with physical exertion (*Alomari et al., 2021*). Symptoms for middle aortic coarctation differ and include – refractory hypertension, abdominal angina, and lower extremity claudication (*Price et al., 2013*).

Conclusions.

1. Although aortic coarctation usually presents in infants prior to the age of one year, it can also be diagnosed in adulthood, but the cause and pathogenesis of aortic coarctations are unclear.
2. It is important to know the symptoms that can indicate this vascular defect.
3. More research should be done to understand the causes of the narrowing so they can be prevented in adults.

Authors Index

A

Atiya, Noy 5

B

Banceviča, Lilija 7

Bodniece, Zane 9

Boikova, Veronika 11, 20

Bozzotto, Elisa 12

G

Gasiņa, Liena 14

Goldiņš, Niks Ričards 16

Grabčika, Arta 17

J

Junusova, Egija 24

K

Kipp, Frederik 19

Koliste, Krista 20

Krauβ, Anna 34

L

Lohova, Elizabeta 22

M

Makarova, Angelina 24

Mardin, Patricia Melike Lucia 25

Muravjova, Jekaterina 27

P

Puriņš, Roberts 28

S

Semjonova, Anastasija 27

Semke, Daniel 30

Ševčenko, Anastasija 37

Siņicins, Ivo 31

Skultecka, Marija 33

Smirnova, Jeļizaveta 34

Strautmane, Estere 35

Strīķe, Luīze Līva 25

U

Unzule, Laima 38, 40

V

Vimba, Paula Marija 42

Z

Zelmene, Una 9